CHAPTER 4

Preparation and Characterization of Semiconductors

NATHAN S. LEWIS
California Institute of Technology
Pasadena, California

MARY L. ROSENBLUTH
Stanford University
Stanford, California

1 Preparation of semiconductors 100
 1.1 Growth of single crystals 100
  1.1.1 Bulk samples of crystalline semiconductors 100
  1.1.2 Crystalline epilayers 102
  1.1.3 Polycrystalline semiconductors 104
  1.1.4 Growth of colloidal semiconductors 105
 1.2 Etching, polishing, and forming ohmic contacts to semiconductors 106
2 Characterization of semiconductor materials 108
 2.1 Orientation of exposed crystal planes 108
 2.2 Bulk electrical and optical properties 108
  2.2.1 Optical properties 108
  2.2.2 Electrical properties 109
 2.3 Surface characteristics 110
 2.4 Flat-band measurements of semiconductors 111
  2.4.1 Mott–Schottky measurements 111
  2.4.2 Flat-band determination with photocurrent–voltage curves 113
  2.4.3 Flat-band determination by high illumination intensity 113
  2.4.4 Flat-band determination by electroreflectance 114
  2.4.5 Flat-band determinations on colloidal semiconductors 114
 2.5 Methods for measurement of the minority carrier diffusion length 114
  2.5.1 Surface photovoltage 115
  2.5.2 Diffusion length from spectral response data 115
  2.5.3 Other methods for diffusion length measurement 115
 2.6 Measurement of surface effects on junction properties 116
  2.6.1 Surface recombination velocity 116
  2.6.2 Trap cross sections and densities 117
  2.6.3 Sub-band-gap photocurrent response 118

3 Summary 118
4 References 119

1 PREPARATION OF SEMICONDUCTORS

1.1 Growth of Single Crystals

Although commercial suppliers can often provide high-quality single crystals of a variety of semiconductors, some experiments require a sample to be grown to certain specifications that are not available commercially. In such instances, crystal growth in the laboratory must be employed. Crystal growth is still somewhat of an art form, and many techniques require extremely skilled operators and expensive equipment if samples of high perfection are to be obtained. The various methods of crystal growth are discussed below. We first discuss growth procedures for bulk semiconductor samples, then for epitaxial layers of material, and finally, summarize methods of fabrication of colloidal photocatalyst systems.

1.1.1 Bulk Samples of Crystalline Semiconductors

Although many techniques are available for the growth of bulk crystalline material, the most common techniques are based on the Czochralski method [1], the float zone method [2], or the Bridgman method [3]. Each technique is discussed briefly below.

The Czochralski (CZ) growth method is the most common procedure for fabrication of Si single crystals [4]. In this method, a crystalline seed is slowly pulled from a melt of extremely pure polycrystalline material. The orientation of the freezing melt at the interface is controlled by the orientation of the seed crystal. Incorporation of dopant atoms is accomplished by addition of the impurity atom to the melt. The dopant density in the final crystal, known as a boule, is a function of the impurity concentration in the melt and the distribution coefficient for the impurity into the boule. Generally, the stoichiometry of the melt will change as the boule grows, so additional semiconductor or dopant material must be continually fed into the melt. Group V elements tend to dissociate from III–V compounds during growth, and these semiconductor boules are encapsulated in boron nitride or liquid B_2O_3 during growth to minimize departures from stoichiometry. Twelve-inch-long, 8-in-diameter crystals of very high purity and minority carrier lifetime can be grown by the CZ method; however, impurities from the melting pot, which is often made of graphite or quartz, are hard to eliminate completely. Crystals that have been grown using the CZ technique include Si, InP, and GaAs.

The float zone (FZ) technique [2] allows fabrication of single-crystal samples with even longer carrier lifetimes than CZ-grown samples. In this method, a polycrystalline bar is locally heated to melting temperature. A single-crystal seed is situated at one end of the vertical bar, and as the molten zone traverses the semiconductor bar, the bar becomes crystalline. Traditionally, heating is done by inductive radio-frequency (RF) irradiation, but this is being supplanted by focused electron beams or optical sources such as xenon arc lamps and lasers. No crucible is required to maintain the shape of the molten zone, because of the surface tension of the semiconductor and leviation effects from the RF field. During the recrystallization process, impurities whose segregation coefficients are less than 1 (i.e., less soluble in the solid than in the melt) are pushed to the ends of the bar. The ends of the bar are then discarded, yielding a sample of very high purity. Also, since no crucible is

required, oxygen contamination is reduced by a factor of 20 to 100 compared to CZ-grown crystals. This is especially important for obtaining long-lifetime Si. Dopant impurities are incorporated either by starting with doped polycrystalline material or by growing the crystal in the presence of a gaseous form of the dopant. The FZ technique has been used mostly for growth of refractory oxides, such as ferrites, aluminates, titanates, and silicates, since the technique is convenient for materials of high melting temperatures.

Some of the III–V and II–VI compounds are difficult to grow by the CZ or FZ methods, because of the high dissociation pressures of the anions. In the Bridgman technique [3], the polycrystalline material is enclosed in a rigid ampoule. This ampoule is then lowered from a furnace that is held at the melting temperature of the material, passed through a baffle, and lowered into a cooler furnace. Depending on the shape of the container, the melt can initially be made to crystallize in a number of different orientations. If the vapor pressure of the melt is too high, this technique may be unsafe, in which case the horizontal Bridgman technique is more suitable. The melt and a seed rest in an open crucible that is pushed from the higher-temperature furnace to the lower-temperature furnace. To raise the partial pressure of the material which is most likely to dissociate, a sample of the pure material is also placed in the furnace. The Bridgman technique has been most popular for growth of II–VI materials such as CdSe, CdTe, ZnSe, and ZnS.

Generally, in the growth methods described above, a background concentration of dopant material is incorporated into the crystals during growth. However, to make structures for electronic devices, it is often necessary to dope the material after growth. This doping process generally consists of two separate steps: deposition and drive-in. First, either a compound containing the impurity, or the impurity itself, is deposited onto the surface of the semiconductor. The source for this deposited material can be solid, liquid, or gaseous. Gas is the source of choice for most wafer manufacturers, because the gaseous flux can easily be regulated through control over the temperature of the furnace, the exposure time, and the flux of the inert carrier gas. During the drive-in step, the furnace temperature is increased, and the deposited impurities diffuse into the sample. The concentration profile of the impurity as a function of time and temperature can be calculated readily from Fick's law for diffusion, provided that the diffusion coefficients are known for the materials of interest. Generally, the higher the temperature, the quicker the drive-in process, and the greater the equilibrium concentration of dopant atom. If the concentration of deposited impurity atoms at the surface is effectively infinite, the resulting impurity profile after the drive-in process is well represented by a complementary error function. A finite quantity of deposited dopant atoms results in a Gaussian impurity profile after diffusion.

A more well-controlled method of dopant introduction can be obtained by ion implantation from a plasma source [5]. In this technique, the semiconductor sample is bombarded with high-velocity ions of the desired impurity. The resulting impurity profile is Gaussian, and the penetration depth depends on the velocity of the ions. Advantages of this method over diffusion are that it can be performed at lower temperatures, and the concentration and depth are easily controlled. Unfortunately, the bombardment process creates structural defects and these have to be removed by thermal or pulsed laser annealing. Also, the implantation depths are shallow compared to other doping processes.

The most uniform doping process is neutron transmutation bombardment; for example,

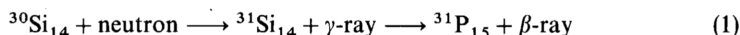

$$ {}^{30}\mathrm{Si}_{14} + \text{neutron} \longrightarrow {}^{31}\mathrm{Si}_{14} + \gamma\text{-ray} \longrightarrow {}^{31}\mathrm{P}_{15} + \beta\text{-ray} \qquad (1) $$

The doping concentration is uniform throughout the sample, because the penetration

depth of neutrons is on the order of a meter. Another advantage is that the process does not require annealing. Unfortunately, it does require a neutron source, which is not standard laboratory equipment.

One caveat about doping is that it may not always be possible to achieve the desired resistivity in a particular semiconductor. This is because intrinsic defects, such as vacancies, can be shallow donors or acceptors. In some samples, the equilibrium concentration of these defects is in excess of any practical dopant concentration. Amphoteric impurities tend to compensate for other added impurities and lead to a limit on doping, because the crystal will lose its structure after a certain critical impurity level has been reached. However, compensation can be useful for deliberately preparing semi-insulating material, which is desirable in a variety of electronic device structures (such as field-effect transistors) [6].

1.1.2 Crystalline Epilayers

Often, only a thin layer of photoactive semiconductor is needed, and epitaxial growth of the semiconductor layer on an inert substrate is sufficient. For certain materials, the purest known samples have been obtained by epitaxial growth techniques. Additionally, certain orientations of the exposed crystal surface have been prepared only by epitaxial growth techniques. In general, an epitaxial layer can be grown on a substrate that is (1) the same semiconductor but of different purity, (2) a different semiconductor, or (3) an insulator or metal. Two common problems in all epitaxial growth procedures are lattice matching between the epitaxial layer and the substrate, and the minimization of the activation energy for carrier transport between the epilayer and the substrate, if current flow in this direction is required. Some of the more common epilayer growth techniques are described below.

The term vapor-phase epitaxy (VPE), also known as chemical vapor deposition (CVD), encompasses a wide range of growth techniques [7]. The popularity of VPE is due to its flexibility in terms of growth conditions and its suitability for wide-scale commercial growth. Some variations that are currently being studied include low-pressure VPE and low-gravity VPE. Common to all these methods is that the semiconductor source material is transported to the substrate surface in a gaseous form. This occurs either by convection, a temperature gradient, or a flux in an inert carrier gas. Since dislocation free growth is usually the goal, the substrate is heated to increase atomic surface diffusion. Also, to enhance nucleation, the substrate is oriented 2 to 3° away from a crystallographic direction, because nucleation occurs preferentially at kinks and step sites. Doping is usually achieved during growth. Multiple layers with reasonably abrupt interfaces can be grown, but crystalline quality deteriorates with thickness.

There are four basic thermochemical growth reactions that can occur in VPE: disproportionation, chemical reduction, pyrolysis, and oxidation [7]. Disproportionation consists of two steps. First, the initial reactant undergoes a chemical reaction at high temperatures to produce a gaseous form of the reactant, for example,

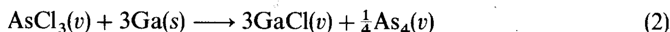

$$AsCl_3(v) + 3Ga(s) \longrightarrow 3GaCl(v) + \tfrac{1}{4}As_4(v) \qquad (2)$$

This reactant gas dissociates at lower temperatures, so the desired element is then available for growth on the substrate. In the case above,

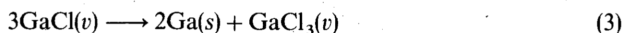

$$3GaCl(v) \longrightarrow 2Ga(s) + GaCl_3(v) \qquad (3)$$

The total reaction is

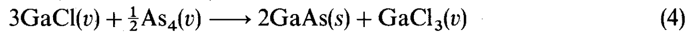

$$3GaCl(v) + \tfrac{1}{2}As_4(v) \longrightarrow 2GaAs(s) + GaCl_3(v) \quad (4)$$

The efficiency of disproportionation is generally low, because the yields of the two reaction steps are poor. Also, the heating system of the furnace must be very complex.

Another form of disproportionation is called pyrolysis. The reactant material, either a hydride or a metallo-organic compound, dissociates at high temperatures. An example of a pyrolytic reaction is

$$SiH_4(v) \longrightarrow Si(s) + 2H_2(v) \quad (5)$$

Pyrolysis is technologically the most important form of VPE, because the reactants are free of undesirable halides and are generally less toxic than the species involved in disproportionation reactions. Also, the temperature of growth can be relatively low. The limitation of this technique has been the cost and availability of high-quality reactants. Metallo-organic vapor-phase epitaxy (MOVPE or MOCVD), which generally utilizes metal alkyls as reactants instead of metal hydrides, has become very popular recently because of the flexibility of the growth process, the reasonable vapor pressures, and the fact that the hydrides of many elements are not stable.

Chemical reduction is simply reduction (usually by H_2) of a reactant gas at elevated temperatures. The reactant gas is often the halide of the desired element. A common example is the VPE growth of Si:

$$SiCl_4(v) + 2H_2 \longrightarrow Si(s) + 4HCl \quad (6)$$

This growth technique yields uniform epilayers at high growth rates, but the growth temperatures are restricted. Of course, the reverse reaction of chemical reduction is oxidation or hydrolysis. This is used to form many oxide films. Unfortunately, oxidation of many reactants occurs too readily, so amorphous films are formed or oxidation occurs in the feed system. Sublimation can also be considered a form of VPE, but no chemical reaction occurs in the process.

If the epitaxial process involves growth from solution as opposed to a vapor phase, it is known as liquid-phase epitaxy (LPE) [8]. Basically, the substrate material is exposed to the reactant solution until the desired epitaxial thickness has been achieved, and then the remaining solution is removed by gravity or by mechanical means. LPE differs from CZ growth because the source solution is not simply the melted semiconductor, but the reactants dissolved in a suitable solvent. With binary compounds, the solvent is usually one of the components, and it is saturated with the other component. This solution is brought into contact with the substrate, and the temperature of the solution is lowered until it is supersaturated. The desired compound then precipitates on the substrate, leading to a concentration gradient of the dissolved species. In a simple model, the rate of growth is controlled by the diffusion of the mass-transport-limited species. Multilayer compounds can be grown by sequential exposure of the substrate to different solutions, with mechanical scraping of the surface between growth steps. To ensure exposure of the substrate to solutions that are saturated but not supersaturated, the substrate wafer is usually preceded by a source wafer, which keeps subsequent solutions at equilibrium conditions. Generally, LPE-grown layers tend to be less smooth than those grown by

VPE. Also, mechanical scraping of the surface after growth tends to contaminate the layers. However, LPE has proved to be more suitable for large-scale growth of multilayer structures such as $Al_xGa_{1-x}As/GaAs$ lasers. In these devices, LPE has demonstrated low defect densities in the epitaxial layers and an extremely high rate of reproducibility in the growth process.

In molecular-beam epitaxy (MBE) [9], the semiconductor source material or the elemental components are evaporated or sputtered (see below) in ultrahigh vacuum and are then directed by a series of orifices and shutters to the substrate. MBE can be distinguished from evaporation or sputtering by the different growth kinetics for the three processes. In MBE, the effusion of material from the source is slow compared to the possible growth rate of the crystal, and the effusion rate can be calculated from thermodynamics. Typically in MBE, the substrate is not purposefully misoriented, and the sample is grown monolayer by monolayer. Thus MBE potentially allows fabrication of atomically smooth layers of very high purity, depending only on the atomic sources and types of vacuums attainable in the chamber. MBE is most appropriate for heterostructures and quantum well devices, where interfaces should be as atomically abrupt and free of defects as possible. Since the system is under ultrahigh vacuum, various analytical devices, such as mass spectrometers, Auger spectrometers, ion bombardment sources, and electron diffractometers, can be used to characterize the epilayer in situ during growth. A potential commercial disadvantage of MBE is the relatively slow growth rate compared to that in other epitaxial growth methods.

1.1.3 Polycrystalline Semiconductors

Although single crystals provide the most reproducible and controllable starting point for photoelectrical investigations, much effort has been devoted to the study of polycrystalline semiconductor samples. Generally, polycrystalline samples are much cheaper and easier to grow than single-crystal samples. They could be more economical as photocatalytic materials if their solar energy conversion efficiencies were to become comparable to those obtained from good single-crystal systems. Some methods for growing polycrystalline semiconductors are described below.

All the single-crystal epitaxial growth techniques mentioned in the section above are capable of generating polycrystalline samples if the growth conditions are varied. Generally, the further the growth interface is from a state of equilibrium, the greater the possibility of polycrystalline growth. Therefore, the degree of polycrystallinity depends on the lattice matching between the substrate and the epitaxial layer, the morphology of the substrate, the temperature of the substrate, the energy of the reactants, and the rate of arrival of the reactants to the surface. Ideally, for more perfect crystals, the rate of nucleation should be much less than the rate of crystal growth.

Electrochemical growth of semiconductors has become popular because of the potential opportunities for large-scale growth [10]. The procedure can be scaled up quite easily, and it is a particularly attractive possibility for research use in a chemistry laboratory. For example, semiconducting oxides can often be grown by oxidation of the relevant metal electrode (i.e., $Ti + O_2 = TiO_2$). It is also possible to precipitate some semiconductors by sustained cathodic current in the appropriate electrolyte plating solutions.

Photocatalytic materials that have been grown by the cathodic current method include CdTe, Si, CdS, GaAs, and InP. Growth parameters include stirring rate, solution concentrations, and electrode overpotential. Growth of a binary compound, AB, for instance, requires deposition of A and B at equal rates, so the concentrations in solution,

[A] and [B], must be adjusted according to

$$E^{\circ}(A^{+}/A) + (RT/n_eF)\ln[A] + \eta_A = E^{\circ}(B^{+}/B) + (RT/n_eF)\ln[B] + \eta_B \quad (7)$$

where E° is the standard electrochemical potential, η the overpotential, $RT/F = 0.0259$ V, and n_e the number of equivalent electrons involved in the deposition reaction. Doping is difficult by this method. As yet, the samples generally have not been of high purity and quality compared to those obtainable by alternative growth methods. However, annealing has been shown to improve the crystallinity in some cases, and further chemical treatment has been utilized in many cases to mitigate the deleterious photocatalytic effects of small grain size or high impurity content in some polycrystalline samples.

Two other methods for growing thin layers of polycrystalline material are evaporation and sputtering. During evaporation, the material of interest is resistively heated in a tungsten or graphite boat, and the solid deposits onto the cold substrate. Sputtering is a very similar process, but the negatively biased material is ejected from the sputtering source by bombardment with positively charged ions. Both methods require an evacuated chamber, and the degree of crystallinity of the semiconductor depends on the heating of the substrate, the vacuum pressure of the chamber, and the speed of preparation. At high growth rates and low substrate temperatures, the film will be amorphous. Outgassing from the reactor walls often leads to impurity incorporation, which, if not controlled, produces lower carrier lifetimes than other growth methods. It is very difficult to grow binary or ternary compounds using these methods, except under well-controlled growing conditions; thus the popularity of these methods results from their experimental simplicity.

Pressed polycrystalline semiconductor disks can be made by sintering the powder at high temperatures and pressures [11]. Often, the sample must be thermally annealed after pressing, in a reducing atmosphere, such as 90% N_2 + 10% H_2. This helps to tie up dangling bonds that may reduce carrier lifetimes. Sintering has the advantage that the geometry and doping density of the sample are easily controlled.

In general, each of the methods above has advantages for a particular semiconductor, depending on whether cost, experimental simplicity, sample purity, abruptness of interfaces, or other sample properties are of primary concern. Numerous books deal with instrumentation and experimental methodology of the growth steps for specific semiconductor materials [1–12], and the reader is referred to these sources for further information regarding a photocatalyst system of particular interest.

1.1.4 Growth of Colloidal Semiconductors

Colloids are prepared by as many different methods as there are colloids. Many of the colloidal oxides are made by hydrolysis of the metal halide. For example, TiO_2 can be made by acidic hydrolysis of $TiCl_4$, and iron oxide results from boiling $FeCl_3$ in water. If the reactant material is a halide, it is recommended that the solutions be dialyzed in H_2O for a few days to diminish complicating factors due to surface modification or residual halides in solution. More attractive methods eliminate the presence of halides altogether, such as using titanium tetraisopropoxide or $Fe(NO_3)_3$. Stabilization requires adjustment of pH (low pH for TiO_2 and pH 7 to 8 for Fe_2O_3) or possibly a stabilizing agent such as polyvinyl alcohol (which is also a hole scavenger).

Metal sulfides, which are common colloidal photocatalysts, are usually made in one of two different ways. They can be prepared either by filtering and washing a preparation of Na_2S that has been added to a solution of the metal salt, or by bubbling H_2S through an aqueous metal ion solution. In either of these methods, sodium hexametaphosphate can be

employed as the stabilizing agent. Doping is achieved by addition of the desired ions to the metal ion solution. With preparation of metal sulfide colloids by precipitation, one must make sure that no unreacted ions remain in solution.

Platinum, which is a good electron transfer catalyst, can be deposited onto colloids by photoplatinization of H_2PtCl_6. RuO_2 is an efficient hole and electron transfer catalyst, and it is deposited by photodeposition from RuO_4 or by hydrolysis of $RuCl_3$ followed by calcination at > 300 °C. Other methods [13] for colloid and metal catalyst preparation are detailed in subsequent chapters of this book, and the reader is referred to these chapters for specific information on other photocatalyst colloids.

1.2 Etching, Polishing, and Forming Ohmic Contacts to Semiconductors

Because surface quality is crucial for attainment of controlled interface properties, etching and polishing of the semiconductor surface is often a key step in semiconductor preparation. The preliminary mechanical polish involves rubbing the semiconductor in a series of particle slurries of successively smaller abrasive particles. Alumina particles that range down to 0.05 μm in diameter are commonly available and inexpensive to use. More expensive diamond particle slurries are often used for finer polishing. Mechanical polishing generally removes macroscopic defects and yields an optically reflective surface.

Unfortunately, a mechanical polish generally does not remove electrical traps on a microscopic level, and it should be followed by a chemomechanical etch. A variety of etchants can be used for common semiconductors, and the appropriate one will depend on the desired final surface properties. Some popular etchants for common semiconductors are listed in Table 4.1. Further detail can be found in current sources on semiconductor photoelectrochemistry [14] as well as in numerous books and reviews of semiconductor processing procedures [15, 16].

Some specialized semiconductor etching procedures are especially relevant to photocatalyst preparation. Certain etches have been used to identify exposed crystal planes and to reveal specific crystal faces. Examples of this technique include the use of 1:100 H_2SO_4/H_2O with 0.08% (by weight) Cr_2O_3 to differentiate between the (0001)A and (0001)B faces of CdS, and the use of KOH–isopropanol–H_2O solutions to expose (111) planes of Si on the (100) crystal face [17]. Similar procedures can be used to create matte-textured surface in order to lower optical reflectivity losses at semiconductor–liquid interfaces. *n*-GaAs etched in stationary 1:1 H_2O_2/H_2SO_4 [18], and *p*-InP etched in 1:2:2 $HCl/HNO_3/H_2O$ [19] are examples of this application. Etching can also be used to measure defect densities. Many etchants preferentially attack the semiconductor at defect sites, and quantification of the number of etch pits by optical or electron microscopy yields the defect density of the sample of interest. A related procedure is photoelectrochemical

TABLE 4.1 Etchants for Semiconductors

Semiconductor	Etching Procedure
Ge, Si, a-Si:H	10% aqueous HF for 10–30 s; H_2O rinse
GaAs, InP	4:1:1 $H_2SO_4/H_2O_2/H_2O$ for 10 s or 0.05–1.0% Br_2 in CH_3OH
CdTe, CdSe	1.0% Br_2 in CH_3OH followed by 0.6 *M* $Na_2S_2O_7$ in 2.5 *M* KOH at 100°C
CdS	Conc. HCl for 10 s; H_2O rinse
GaP	Hot 1:1 HCl/HNO_3 for 5–10 s
MoS_2	Peel van der Waals plane with tape
TiO_2, $SrTiO_3$	Hot conc. H_2SO_4 (250°C)

etching, in which the electrical trap sites capture the photogenerated carriers, and these sites are then etched preferentially. Photoelectrochemical etching has been used in a number of instances to improve the junction properties of single-crystal and polycrystalline semiconductors in contact with liquids [20].

When working with semiconductor electrodes, it is important to obtain good electrical contact to the sample under study. Often, this cannot be achieved simply by soldering a metal lead to the back of the sample, because the contact will be electrically rectifying. The proper contact must have a low resistance under both forward and reverse biases and should be stable with temperature cycling and with time. Theoretically, metals with high work functions should form good ohmic contacts to *p*-type samples, and metals with low work functions should be useful for *n*-type contacts. For instance, In forms a good ohmic contact to *n*-Si, and Au is a good contact material for *p*-Si [6]. Unfortunately, the rule can be applied rigorously only to ohmic contacts of semiconducting oxide materials. This is because the uncertainties relevant to Schottky barrier height prediction on covalent semiconductors also make it difficult to predict ohmic junction formation. The most practical approach is to adopt procedures for ohmic contact formation found in the literature. Ohmic behavior should always be verified by I–V measurements on the sample–contact assembly under investigation. Some ohmic contacts for common semiconductor materials are summarized in Table 4.2.

For some semiconductors, the only practical route for making ohmic contacts is to form a junction through which carriers can readily tunnel. If the back surface of the semiconductor is doped to degeneracy, majority carriers will easily tunnel through the thin barrier, and a wide variety of metals will make an ohmic contact. Doping of the back surface is also useful for enhancing the minority carrier diffusion length [21]. This back surface field reflects minority carriers from the high recombination region of the back contact back to the front surface. Back surface fields have been used to make minority carrier diffusion lengths in bulk Si and epitaxial GaAs samples comparable to the thickness of the photoactive semiconductor layer.

Low-resistance contacts are also desirable for metal catalyst–colloidal semiconductor junctions. Very few systematic studies of the barrier properties of these junctions have been performed to date; however, one investigation suggested that Pt forms an ohmic contact to CdS colloids, even though it forms Schottky barriers with single-crystal CdS [22]. This might be possible because of the much higher density of interface states in the colloidal

TABLE 4.2 Ohmic Contacts for Semiconductors

Semiconductor	Ohmic Contact
n-Si	Rub on Ga/In alloy
p-Si	Evaporate Al, then anneal at 450°C under H_2
n-GaAs, *n*-InP	Evaporate Au/Ge (88:12) alloy, then anneal at 400°C under forming gas
p-GaAs, *p*-InP	Evaporate Au/Zn (99:1) then anneal at 350°C under forming gas
n-MoS_2	Ag epoxy
n-CdS, *n*-CdSe, *n*-CdTe, *n*-Fe_2O_3, *n*-TiO_2, *n*-$SrTiO_3$	Rub on Ga/In alloy
n-GaP	Evaporate Au/Ge (88:12) alloy, then anneal at 400°C under forming gas
p-CdTe	Diffuse Li, then evaporate Au and anneal

Source: Ref. 14.

systems. Such damaged junctions could act as excellent majority carrier shunts to yield ohmic electrical behavior. An alternative explanation is that during photoelectrolysis, H_2 gas exposure lowers the work function of Pt to a point where the barrier height is so low that an ohmic contact with the CdS particle is formed [23]. In general, the physics and chemistry of metal–colloidal semiconductor interfaces require further investigation.

2 CHARACTERIZATION OF SEMICONDUCTOR MATERIALS

In this section we describe common experimental methods that have been used to characterize semiconductor materials. We discuss techniques for identifying the orientation of the sample, for determining bulk electrical properties, and for characterizing the chemical composition and physical structure of the surface. We then discuss measurement procedures of relevance to the photo-generated current properties of the system, including the minority carrier lifetime, the surface recombination velocity, and the flat-band potential. Characterization of semiconductor colloidal particles is not discussed, because the relevant techniques are discussed in subsequent chapters.

2.1 Orientation of Exposed Crystal Planes

The most common methods for the identification of the orientation employ the ability of crystals to diffract x-rays. The periodic spacing of the atomic lattice acts like a diffraction grating. If the unit cell structure is known, the spacing, symmetry, and intensity of the diffraction pattern can be used to determine the crystal orientation [24]. This procedure is always reliable and can be used whenever information on the exposed surface is needed.

Another method for the determination of crystal orientation is to take advantage of the selectivity of certain etches toward specific crystal faces. For example, a (111) GaAs face will respond differently from a $(\bar{1}\bar{1}\bar{1})$ face in the presence of an etch that removes As. Preferential etches have been discovered only for some semiconductors and for certain crystal faces, so the technique is of use only in specific systems. However, the technique has the advantage that visual inspection of the surface suffices to make an identification of the exposed crystal. For certain semiconductors, an alternative to chemical etching is the use of electron spin resonance techniques [25]. Different faces of a crystal will have different densities of dangling bonds at the interface. Depending on the reconstruction of the surface, ESR can measure differences between faces due to these dangling bonds. For instance, Si(111) faces have been shown to exhibit a different spin anisotropy than Si(100)-oriented faces [25].

Often, the current–voltage characteristics of two different faces of an identical semiconductor can be vastly different [14]. This is because of the variation in work function, surface-state density, and atomic reconstruction for the different crystal faces. For example, the (111) face of GaAs, which is a close-packed plane of Ga atoms, behaves very differently from the $(\bar{1}\bar{1}\bar{1})$ face, which is a close-packed plane of As atoms [26]. Also the bulk properties of the semiconductor, such as carrier mobility, may be anisotropic. Thus it is often crucial to specify the orientation of semiconductor samples using one of the techniques described above.

2.2 Bulk Electrical and Optical Properties

2.2.1 Optical Properties

The most important optical characteristic of a semiconductor is its band gap. The optical absorption spectrum yields precise information on this important parameter. For a direct

gap, a plot of α^2 versus $h\nu$, where α is the absorption coefficient, will give the band gap as the x-intercept [27]. If the gap is indirect, a plot of $\alpha^{1/2}$ versus photon energy will have two linear regions, one corresponding to absorption with phonon emission and one corresponding to absorption with phonon capture. The average of the two intercepts is the energy of the indirect band gap. One-half of the difference between the two intercepts is the phonon energy required for band-gap excitation.

Optical absorption properties are also of importance in determining the photon penetration depth versus wavelength. For the longer wavelengths, transmission through a certain thickness, d, of sample will yield the absorptivity according to the equation

$$\Gamma_{\text{trans}} = \Gamma_0 \exp(-\alpha d) \tag{8}$$

where Γ_0 is the incident intensity and Γ_{trans} is the transmitted light intensity. At the shorter wavelengths, the transmission can be measured through thin semiconductor layers grown on a transparent substrate. An alternative method for determining the absorption coefficient versus wavelength is to determine the real and imaginary parts of the refractive index from reflectance, transmittance, or ellipsometric data, and then to use the Kramers–Kronig relationship to determine the absorption coefficient of the solid over the wavelength region of interest [28].

2.2.2 Electrical Properties

Some of the important electrical properties of semiconductors include the free carrier concentration, the sample conductivity, the carrier mobility, and the intrinsic carrier concentration. Methods for measurement of these parameters are discussed in this section.

To measure the conductivity of the sample, a four-point probe determination of the sample resistance is typically performed. A four-point probe measures the voltage drop between two inner probes when a known current is passed between two outer probes. This will give the resistance/unit area of the sample, which can be converted to resistivity if the thickness of the sample is known. The four-point probe measurements provide very convenient and reliable methods for determining sample conductance. A related quantity is the sheet resistance, ρ/d, of a square of material. The sheet resistance is important for work with thin films, since transport parallel to the exposed face will occur with relatively large resistive losses.

If the conductance is known, the free carrier concentration can be obtained using the relationship $\sigma = ne\mu$. The value of the mobility must be determined from other experimental data, because the mobility is somewhat dependent on the dopant density of the semiconductor. However, a good first approximation to the free carrier concentration often can be obtained by using a representative value of the mobility for the particular type of semiconductor of interest. For Si and GaAs, accurate values of the mobility versus resistivity have been compiled in the literature [29], and these data are quite useful in routine laboratory measurements. It is also important to note that the dopant density, or impurity density, is in general different from the free carrier density, because not all of the dopants are ionized in many semiconductors at room temperature.

Both the net majority carrier concentration and the majority carrier mobility may be measured with a Hall probe. The Hall technique is based on the fact that in the presence of a magnetic field, the motion of electrons sets up an electric field which is in the opposite direction to one that would be induced by holes. Van der Pauw has generalized the experimental procedure so that the characteristics of a sample of any shape or size can be measured [30]. Discrepancies between the measured mobility and net carrier

concentration give an indication of the gross concentration of nonionized impurities in the sample.

Another well-known method for measuring carrier mobilities is the Haynes–Shockley technique [31]. A pulse of excess carriers is generated optically near one end of a semiconductor bar of length d. An electric field is applied, so the excess carriers drift to the other end of the bar, creating a drift current. Current ceases when the excess carriers reach the other electrode. The time delay of this drift current is given by $d/\mu\mathscr{E}$. By changing the polarity of the bias, the mobilities of both the minority and majority carriers can be measured. A classic investigation using this technique was performed by Haynes and Shockley, who measured both the minority carrier lifetimes and the minority carrier mobilities of various samples of Ge [31].

The intrinsic carrier concentration in a semiconductor can be determined from the density of states in the conduction and valence bands, and the energy gap, according to

$$n_i^2 = N_c N_v \exp(-\mathbf{E}_g/kT) \tag{9}$$

A rough approximation that can be used for many materials is to assume that $N_c = N_v = 10^{19}\,\text{cm}^{-3}$ and to use the relationship (9). Theoretical calculations of N_c and N_v from tight binding theory have proved very successful in some cases. N_c and N_v are also theoretically measurable by photoemission. A more direct experimental method to determine n_i is to heat the semiconductor to temperatures far above temperatures where all impurities are expected to be ionized. Then the concentration of thermally generated carriers will exceed the concentration of extrinsic carriers. Thus, at high temperatures, $n = p = n_i$, and n_i can be measured directly by Hall or conductivity measurements. As a check on the value, measurements at several different temperatures are recorded, and the dependence of n_i on temperature should be exponential and in accord with the known value of $\mathbf{E}_g$. Experimental measurements and calculations of n_i show a definite correlation to band-gap energy.

2.3 Surface Characteristics

The full arsenal of standard surface analysis techniques [32] has been applied to many semiconductor surfaces, and space does not permit a detailed discussion of all known information about the properties of semiconductor surfaces. Accordingly, we outline briefly some of the more common techniques and will highlight their major applications.

At a molecular level, the surface can be characterized by x-ray photoemission spectroscopy (XPS), Auger spectroscopy, low-energy electron diffraction (LEED), scanning tunneling microscopy (STM), scanning electron microscopy (SEM), and transmission electron microscopy (TEM). LEED is appropriate when it is known that the surface is very well ordered. LEED yields information concerning long-range periodic structure in the near-surface region [33]. The low-energy electrons are diffracted off the first few monolayers, and the diffraction pattern gives information about symmetry of the surface. STM, although relatively new [34], is being used frequently to characterize semiconductor surfaces, and is complementary to LEED in that it reveals short-range order on the atomic scale. STM also has the advantage that it can yield information on disordered surfaces or surfaces with mixed phases, whereas LEED only yields information on that portion of the surface that has a long-range periodic structure. In very recent work, STM has been used to identify the location of surface states on Si and GaAs [35] and to determine their binding energies. This could become a very powerful tool if utilized more widely on samples of interest to photocatalysis.

Performing at somewhat lower resolution than STM's sub-angstrom resolution is TEM. Although sample preparation is tedius, high-resolution TEM can yield information concerning the surface morphology, crystallinity, and orientation. For example, data on Si/SiO_2 interfaces can display the registry between the Si and oxide lattices and also allows measurements of interdiffusion during junction formation [36].

Elemental identification and chemical information on surface composition can be obtained by a number of surface-sensitive techniques. XPS is extremely useful in providing a semiquantitative elemental analysis of surfaces and in obtaining oxidation-state information for the surface atoms. Auger spectroscopy is more readily quantified than XPS and is used ordinarily for surface composition information, because oxidation-state information is not as readily extracted. Scanning Auger can be used to probe compositional variations on the surface with a resolution of better than 1 μm, and this is also a feature that is unavailable at present with XPS instrumentation. On a larger scale (1 μm depth and 10^{-8} cm^2 surface area), the near-surface composition can be determined by use of an electron microprobe. Finally, average oxidation state information can be obtained by x-ray absorption measurements, while EXAFS (x-ray absorption fine structure) spectra can yield information concerning inner-shell coordination of the atom of interest [37]. The x-ray techniques are especially useful for in situ measurements on semiconductor–liquid interfaces [38], whereas all the electron and ion spectroscopies discussed above do not have this capability.

To complete our discussion of surface characterization, we must include methods that yield information about the electronic properties of the surface and bulk semiconductor. Perhaps the most important method is ultraviolet photoelectron spectroscopy (UPS) [39], which yields direct information on the band structure of the solid. Additionally, UPS spectra provide information on the surface Fermi-level position. This information, coupled with careful determination of the band bending of the sample, allows assignment of the electron affinity of the solid as well as investigation of Fermi-level pinning properties of semiconductor–metal and semiconductor–gas interfaces. The photoemission techniques have greatly expanded in utility with the recent advent of synchrotron radiation sources, which provide intense tunable beams over the wavelength range of interest for semiconductors. Application of this technique to specific semiconductors is reviewed extensively in the current literature [40].

2.4 Flat-Band Measurements of Semiconductors

In Chapter 3, discussions of the energetics and kinetics of semiconductor–liquid junctions underscored the importance of determining the flat-band potential of the semiconductor. Many techniques have been developed to measure this quantity [14], and some of the more common methods are presented below.

2.4.1 *Mott–Schottky Measurements*

In Chapter 3 we derived an expression for the depletion width, W, of a semiconductor. Assuming that all the dopants are ionized in this region, and using the known value of the dielectric constant for the material, $\varepsilon_s (= k\varepsilon_0)$, we obtain the following expression for the space charge capacitance versus applied voltage of Schottky barrier or a semiconductor–liquid junction:

$$Q = \left[(2qkN_D)\left(V_{bi} + V - \frac{kT}{q} \right) \right]^{1/2} \tag{10}$$

Taking the derivative of Q with respect to V, we obtain an expression for the differential

capacitance, C_d:

$$C_d = dQ/dV = \left[(qkN_D) \bigg/ \left(V_{bi} + V - \frac{kT}{q} \right) \right]^{1/2} \tag{11}$$

Therefore, a plot of $1/C_d^2$ versus V should yield a straight line of slope $2/q\varepsilon_s N_D$ and x-intercept of V_{bi} (or V_{fb}).

Intuitively, eq. (11) makes good physical sense. The more charge that flows when a small, fixed voltage is applied, the bigger the differential capacitance, dQ/dV, will be. Near flat-band, a small change in voltage requires a relatively large amount of charge to be transferred, whereas at large reverse bias, the same amount of voltage does very little to increase the space charge width. Thus, for constant dV steps, dQ should decrease as V is increased, in accord with eq. 11.

The most common procedure for obtaining differential capacitance versus voltage data is to apply a small ac (sinusoidal) voltage in addition to the desired dc potential. The resultant current will have an in-phase and quadrature (90° lag) component, and an analysis of these components yields the cell impedance.

The choice of the equivalent circuit of resistors and capacitors used to represent a semiconductor–liquid junction is crucial to the analysis of the current–phase data. The conventional description of the liquid junction equivalent circuit is represented as follows [41]:

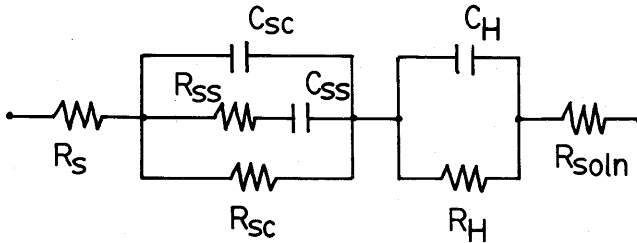

The subscript s refers to the semiconductor bulk, sc to the space charge, ss to surface states, H to the Helmholtz layer, and $soln$ to solution. This circuit is reasonable because there will clearly be a capacitance and resistance for the Helmholtz layer, and the R and C for the semiconductor space charge layer will be in series with the Helmholtz elements. The surface states also have their own capacity and charge transfer resistance, and careful consideration of the situation reveals that these elements should be placed in series with the Helmholtz elements, but in parallel with the space charge elements. Finally, we include the series resistance of the electrode and contact, and the solution series resistance, as distinct resistive components in our circuit.

One possible simplification of this circuit is the following:

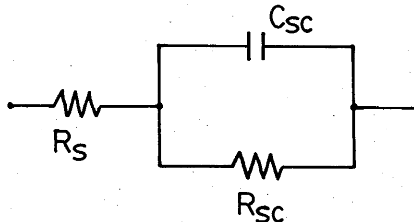

This simplification often can be readily justified. The solution and electrode resistances are combined into one series resistor. If the Helmholtz layer resistance is small, the RC portion of the Helmholtz layer circuit impedance is dominated by C_H. Further more, C_H is usually much larger than the semiconductor space charge capacity, and for capacitors in series, only the smallest capacity matters, so we can neglect C_H. Also, if we assume that the ac impedance measurement is performed at a high-enough frequency that surface states cannot fill and empty on our time scale, these elements do not contribute to charge storage.

At sufficiently high frequencies, the impedance of this simplified circuit can be written as $G = 1/R_s$ and $B = 1/\omega C_{sc} R_s^2$, where G is called the conductance and B is the susceptance (both in units of siemens). $1/C^2$ versus V should be determined at several different frequencies, to verify that the slope and intercept do not change. If they do change, a more detailed analysis using the correct equivalent circuit described above can yield information concerning surface-state densities and energetic locations [42].

2.4.2 Flat-Band Determination with Photocurrent–Voltage Curves

Another method sometimes used in the literature to determine V_{fb} is to analyze I^2 versus V plots taken under illumination. Let us consider monochromatic irradiation of penetration depth α^{-1} on a semiconductor–liquid junction. Assume that the dark current is negligible over the voltage range of interest and that the measured current is the photogenerated current $I_{ph}(V)$. From the Gartner model presented in Chapter 3, we then predict that

$$J_{ph} = \frac{\Gamma_0}{A}(1 - R)\left(1 - \frac{e^{-\alpha W}}{1 + \alpha L_p}\right) \Rightarrow J_{ph} \propto 1 - \frac{e^{-\alpha W}}{1 + \alpha L_p} \quad (12)$$

where J_{ph} is the photocurrent density.

The voltage dependence is, of course, implicit in the dependence of W on V. Rearranging and assuming that $L_p = 0$, we find that

$$\begin{aligned} J_{ph} \propto 1 - \exp(-\alpha W) \simeq \alpha W/2 &\Rightarrow J_{ph} \propto (\alpha/2)(V_{bi} + V)^{1/2} \\ &\Rightarrow J_{ph}^2 \propto [\alpha/2]^2 (V_{bi} + V) \end{aligned} \quad (13)$$

It is clear that this method only works well for semiconductors with extremely small diffusion lengths.

2.4.3 Flat-Band Determination by High Illumination Intensity

Another method often used to determine the flat-band potential is to illuminate the semiconductor with extremely high intensity light and to assume that the bands are flattened. Under these conditions, the measured voltage between the semiconductor and a metal electrode is taken to be a good approximation to the difference between the solution redox potential and the flat-band potential [43].

This procedure has several difficulties. First, referring to eq. 38 in Chapter 3, we see that the dependence of V_{oc} on I_{ph} should be logarithmic, and therefore a plot on linear axes of V_{oc} versus I_{ph} will exhibit a false saturation value. Second, V_{oc} decreases as the cell temperature increases, because all I_0 terms have temperature dependencies of $\exp(-\text{const}/kT)$. Thus the local heating induced by high illumination levels tends to make the measured V_{oc} level off with increased light intensity. The flat-band values obtained using this method will certainly be lower limits on the true flat-band positions, and the measured

values should be confirmed using another technique before a final quantitative value is presented.

2.4.4 Flat-Band Determination by Electroreflectance

Flat-band positions have also been determined by use of the electroreflectance properties of semiconductor surfaces [44]. In its simplest form, the reflectance of a material should increase as the internal electric field increases. Therefore, if the reflectivity is monitored in response to the application of a small ac voltage, a null point indicates the flat-band potential. This occurs because in depletion, the reflectivity should increase in phase with the voltage, because additional reverse bias increases the electric field. In contrast, in accumulation, the reverse bias decreases the electric field and therefore should decrease the reflectivity. At flat-band, on average, the ac reflectivity is therefore a null signal.

However, the analysis of real interfaces is complicated by the presence of excitons and Franz–Keldysh oscillations [44]. These produce other null points as a function of wavelength and dc potential, and make it very difficult to extract the flat-band potential from these data. Electroreflectance spectra have found great use in determining the optical properties of semiconductors, and detailed information on this aspect of semiconductor–liquid junctions is available in the condensed matter physics literature [45]. They have only been applied recently to stable semiconductor–liquid junctions, but show promise in assignment of flat-band positions for sufficiently well-defined electro-optical systems.

2.4.5 Flat-Band Determinations on Colloidal Semiconductors

Obviously, it is difficult to bias an individual colloid particle relative to the solution, so optical methods are often employed to understand the thermodynamics of these particles. One method that has been used to measure the flat-band potentials of colloidal particles is to equilibrate their photogenerated charge carriers with solution redox species of known potential. For example, the flat-band potential of TiO_2 colloids in aqueous solutions has been determined by their ability to reduce methyl viologen, MV^{2+} [13]. The $MV^{2+/+}$ redox potential is pH independent, but the flat band of TiO_2 is known to shift 60 mV with a one unit change in pH [14]. Unter high-level illumination, the energy of the photogenerated electrons is assumed to be equal to the conduction band energy, and the $MV^{2+/+}$ redox potential should equilibrate with this energy level. Therefore, a measurement of the steady-state concentration of MV^+ at various pH values should yield the flat-band potential of the particles. The resulting concentration of MV^+ has been measured in a number of ways: (1) by determination of the redox potential of the solution, (2) by the optical absorption of the solution (since MV^+ is highly colored), and (3) by the oxidation current of MV^+ at an inert electrode in solution. Of course, the flat-band potentials of these colloids might well vary with illumination, because their surface-state densities are expected to be quite large. Other than this electrochemical approach to measurement of E_{fb}, few methods are available for determination of this parameter for colloidal systems.

2.5 Methods for Measurement of the Minority Carrier Diffusion Length

The minority carrier diffusion length is an extremely important parameter of a semiconductor sample. Its value affects the bulk diffusion–recombination limited V_{oc} and also affects the spectral response properties of the solid. Several methods are available for determination of this quantity. In the treatment below, we assume that the semiconductor is *n*-type, so we are therefore interested in measuring L_p.

2.5.1 Surface Photovoltage

The surface photovoltage method is a contactless technique and is the ASTM (American Society for Testing and Materials) method of choice for measurement of diffusion length [46]. The method works well only for Si and indirect gap materials. The basis for the method can be found by reference to a simplification of the Gartner equation, eq. 75 of Chapter 3:

$$I_{ph} = \Gamma_0(1 - R)[1/(1 + 1/\alpha L_p)] \tag{14}$$

Since measurement of the photocurrent requires good electrical contact to the semiconductor, the wavelength response of the photovoltage is determined instead. The voltage response can be followed by capacitively coupling the semiconductor through an insulating dielectric, such as mica, to an optically transparent conducting electrode. Assuming that the light intensity is sufficiently low that we can expand the exponential, we obtain the following expression for the wavelength dependence of the photovoltage:

$$V_{oc} \propto 1/(1 + 1/\alpha L_p) \tag{15}$$

Provided that $L_p \gg W$ and $1/\alpha(\lambda) \gg W$, a plot of (photovoltage)$^{-1}$ versus $1/\alpha(\lambda)$ yields a value for L_p.

2.5.2 Diffusion Length from Spectral Response Data

As discussed in the preceding section, it can be seen that the short-circuit photocurrent can also be used to obtain a measure of the minority carrier diffusion length. Note that this technique is very similar to the surface photooltage method and has the same constraints on its applicability.

For a typical spectral response, the red (long-wavelength) region of the spectrum will show poor quantum yields if bulk recombination (small L_p) is the problem, while the short-wavelength region will show poor responses if the surface leads to large recombination losses. Thus the spectral response data can yield information regarding the effects of surface traps in contact with the electrolyte of interest. An additional advantage of the short-circuit photocurrent measurement is that if there are traps in the bulk that can be saturated, the diffusion length that is measured at low-level illumination may not be the value that applies under higher injection levels. With the short-circuit photocurrent method, we can take this effect into account by measuring the ac photocurrent response (with a lock-in amplifier) from a chopped light source, even in the presence of a steady-state, high-intensity, dc bias light. This is very useful with polycrystalline samples and amorphous materials, which often show different diffusion length values at various injection levels [47]. Analysis of the data is the same at all light levels, because the ac probe light provides a unique frequency for analysis of the photocurrent versus wavelength dependence.

2.5.3 Other Methods for Diffusion Length Measurement

Many other methods for the measurement of the minority carrier diffusion length involve the determination of the minority carrier lifetime, and the subsequent use of the relationship $L = (D\tau)^{1/2}$ to determine the diffusion length. Some of the methods are outlined briefly below. For further information, the text by Many et al. [16] has excellent descriptions of the more esoteric techniques (channel conductance of a field-effect transistor, etc.) and it is also a good source of references for the methods discussed in this chapter.

Basically, any method that can be used to measure the free carrier lifetime after an optical excitation pulse will be useful in determining the minority carrier lifetime. For instance, one can monitor the bulk band-to-band radiative luminescence lifetime under conditions where the surface nonradiative recombination processes are negligible [48]. Another technique takes advantage of the fact that free carriers absorb microwave radiation; thus pulsed excitation of a semiconductor sample inside a microwave cavity will produce a transient increase in microwave absorption, and the absorption decay yields the carrier lifetime [49]. In the transient grating technique, a probe beam is scattered off a grating formed from the free carriers generated by two diffracting beams, and the grating decay time at different grating fringe spacings allows a calculation of the minotiry carrier lifetime [50]. Photoconductivity decay, as measured by the change in resistance between two ohmic contacts mounted at the edges of the crystal, is another method of determining τ_p, and therefore L_p [51].

The last method to be discussed uses electron beam excitation to induce current flow (EBIC). In this technique the carriers are generated by an electron beam, instead of by absorption of a photon, but their drift and diffusion processes are otherwise identical. The advantage of the method is that the electron beam can be focused and used to generate carriers locally over a much shorter absorption depth than is usually attainable with light. Also, the ability to scan the electron beam away from the junction provides a direct probe of the diffusion length of the sample. EBIC is also extremely useful for polycrystalline samples, where the current is expected to vary laterally along the junction plane [52]. EBIC measurements require current to be collected and therefore must be performed either on $p-n$ junctions or, more often, on Schottky barriers.

2.6 Measurement of Surface Effects on Junction Properties

Often, surface states at a semiconductor–liquid junction can control the kinetics of recombination, trapping, electron transfer, stability, and catalysis. Clearly, measurements of surface-state concentrations, energy levels, and capture coefficients are necessary for an evaluation of the semiconductor as a photocatalyst. In this section we discuss some of the more common approaches to characterization of semiconductor surface properties.

2.6.1 Surface Recombination Velocity

As mentioned in Chapter 3, the surface recombination velocity, S, is the rate constant for surface recombination as a function of the injected minority carrier density. The determination of S from semiconductor characteristics requires deconvolution of the bulk characteristics from the surface characteristics. This can be accomplished experimentally either with a change in sample thickness, a change in the probing depth of the measurement perpendicular to the surface, or prior knowledge of bulk characteristics.

In a technique developed by Harten in 1960 [53], the photovoltage that is developed at a Schottky barrier on the back surface of a sample is measured as a function of the wavelength of monochromatic light incident on the front side of the sample. The ability of the photogenerated carriers to diffuse to the back surface will depend on the bulk diffusion length and the recombination rate at the front surface that is in contact with solution. If the front-surface recombination velocity is high, those carriers generated near the front surface will not be able to diffuse to the back Schottky barrier. Therefore, the photocurrent collected at the back will be low. Alternatively, if the penetration depth is large, most of the photogenerated carriers will be collected and the photocurrent will be large. This technique has the advantage that it allows measurement of the surface recombination velocity in situ. Also, S can be measured as a function of surface potential, by applying a

potential between an ideally polarizable electrode in solution and the back-surface ohmic contact.

Often, S is measured by transient techniques [16]. Many of the transient techniques mentioned in the preceding section for measuring minority carrier diffusion lengths can be adapted to determine surface recombination velocities, or equivalently, surface carrier lifetimes. For example, photogenerated carrier decay as measured by microwave absorption is useful for measuring S in both bulk samples and colloids [49]. Either the surface lifetime is so much shorter than the bulk lifetime that the decay is considered entirely due to surface recombination (usually the case for colloids), or else bulk effects are measured independently or solved for by the dependence of the apparent lifetime on the sample thickness. The same analysis can be performed using the decay of photoluminescence (PL) in a sample [48]. If the surface recombination velocity is high and the sample is thin enough for the carrier to reach the surface, photogenerated carriers will recombine quickly, and the time constant for PL decay in a sample will be short. The dependence of the PL lifetime on photon penetration depth and on sample thickness yields sufficient information to determine both the bulk lifetime and surface recombination velocity.

For measurements of S at semiconductor–liquid junctions, one must be careful to separate the effects of surface recombination from the effects of electron transfer into a redox species in solution. For example, if the PL decay of an n-type semiconductor is measured in the presence of a reduced species in solution, it will be unclear whether decay is due to recombination in surface states or hole transfer into solution. However, if S measurements are performed in solution without any redox species, one has to worry about photodecomposition of the interface under illumination. Thus S measurements are difficult at liquid interfaces, and the data must be interpreted with due caution.

2.6.2 Trap Cross Sections and Densities

In Section 2.4.1, surface-state charging was found to be a complicating factor in differential capacity measurements of the flat-band potential. However, these effects can be used to determine surface-state densities and energy levels. When an ac voltage is applied to a junction, the occupancy of a surface state changes drastically when the surface Fermi level moves through the surface-state energy level. The rapidity with which these surface states are able to reach quasi-equilibrium depends on their ability to interact with the conduction band or the valence band. Therefore, measurements of the capacitance of the junction as a function of frequency and voltage have the potential to provide information regarding the number of surface states and their energetic position. The same caveats mentioned above for flat-band measurements by C–V methods apply to measurements of surface-state densities. The equivalent information can be derived from measurements of conductance as opposed to capacitance, and the conductance determination has the advantage that interface state effects do not have to be separated from depletion layer and double-layer effects.

Deep-level transient spectroscopy (DLTS), thermally stimulated capacitance, and thermally stimulated current methods are offspring of capacitance–voltage measurements, but they have the added parameters of temperature and time. Basically, a voltage pulse is applied to a junction, and either the decay rate of capacitance or conductance is measured as a function of temperature. As the temperature is lowered, those interface traps or surface states toward the middle of the forbidden gap will lose their ability to communicate thermally with the bands. So a change in temperature effectively allows study of each trap level independently. The amplitude of the capacitance or conductance

decay is related to the density of interface traps, and the rate of decay provides information about the energies of the traps. The transient decay rate is also affected by variations in capture cross sections, but this effect can be independently followed by changing the width of the applied bias pulse. DLTS is the most promising of these techniques, because the measurements are not affected by the thermal history of the sample.

2.6.3 Sub-Band-Gap Photocurrent Response

Another method for identification of surface-state energy levels involves optical excitation of carriers into or out of the surface state [54]. This process, which requires irradiation with sub-band-gap light, produces photocurrent that can be measured in a conventional cell arrangement. Typically, the surface-state absorption is very small, and modulated light with lock-in detection of current is used to measure the resulting signal. It is necessary to take extreme care in eliminating sources of direct band-gap excitation of carriers at energies below the fundamental absorption edge. A useful method to accomplish this takes advantage of the common decrease in E_g with increases in temperature, so that a heated sample of the same semiconductor material can be used as an optical filter of the incident light. The method has been used successfully to identify surface energy levels on Si, GaAs, and other common semiconductors in contact with liquid electrodes.

For crystalline samples and colloidal systems, luminescence at energies lower than band-gap is a widely used method for the location of surface-state levels. Additional sensitivity can be achieved for surface traps versus bulk defect states by modulating the potential applied to the semiconductor crystal and monitoring the luminescence with phase-sensitive detection techniques. The bulk luminescence should not change as the potential is varied, but the change in depletion width and field strength should effect large changes in the luminescent yield for surface-related carrier recombination pathways. A related set of experiments is electroluminescence, where one carrier is provided by application of the applied potential and the other carrier is obtained by charge transfer from a redox species in solution. These luminescence techniques have been employed quite widely for the study of photocatalysts, and a wealth of information has been obtained regarding surface-state energies, trapping-rate constants, and other important properties of semiconductor–liquid interfaces.

3 SUMMARY

In this chapter we have described the preparation and characterization of photocatalyst materials and have addressed methods for growth of single crystals, crystalline and polycrystalline epilayers of the desired samples, and growth of colloidal systems of photocatalyst particulates. Characterization techniques include surface characterization methods, determination of important optical and electrical properties of the material, and measurement of interfacial quantities such as the flat-band potential. With the theory of Chapter 2 and the present tools for preparation and characterization of semiconductor materials, we can now proceed, in the remainder of the book, to discuss the specific details of photocatalyst behavior in systems of contemporary interest to chemists and physicists.

ACKNOWLEDGMENTS

The authors are grateful to the Department of Energy through its Office of Basic Energy Sciences and to the Office of Naval Research for support during the preparation of this manuscript.

4 REFERENCES

1. (a) G.K. Teal and E. Buehler, *Phys. Rev.*, **87**, 140 (1952).
   (b) A.J.R. DeKak, in *Handbook of Semiconductors*, T.S. Moss and S.P. Keller, Eds., North-Holland, Amsterdam, 1980, Vol. 3.
2. (a) R. Emeis, *Z. Naturforsch. A* **9**, 67 (1954).
   (b) H.C. Theuerer, *Bell Lab. Rec.*, **33**, 327 (1955).
3. L.R. Weisberg, *The Art and Science of Growing Crystals*, Wiley, New York, 1963, p. 381.
4. E. Stirtl, in *Semiconductor Silicon*, H.R. Huff and E. Stirtl, Eds., The Electrochemical Society, Pennington, N.J., 1977, p. 4.
5. J.F. Gibbons, in *Handbook of Semiconductors*, T.S. Moss and S.P. Keller, Eds., North-Holland, Amsterdam, 1980, Vol. 3., p. 599.
6. S.M. Sze, *Physics of Semiconductor Devices*, 2nd ed., Wiley, New York, 1981.
7. (a) G.W. Cullen and C.C. Wang, *Heteroepitaxial Semiconductors for Electronic Devices*, Springer-Verlag, New York, 1978.
   (b) E.G. Schneider and V. Ruth, *Advances in Epitaxy and Endotaxy*, VEB Deutscher Verlag für Grundstoffindustrie, Leipzig East Germany, 1971.
   (c) L. Hollan, *Acta Electron.*, **21**, 117 (1978).
8. J.J. Hsieh, in *Handbook of Semiconductors*, T.S. Moss and S.P. Keller, Eds., North-Holland, Amsterdam, 1980, Vol. 3, p. 415.
9. L.L. Chang, in *Handbook of Semiconductors*, T.S. Moss and S.P. Keller, Eds., North-Holland, Amsterdam, 1980, Vol. 3, p. 563.
10. (a) M. Tomkiewicz, I. Ling and W.S. Oarsons, *J. Electrochem. Soc.*, **129**, 2016 (1982).
    (b) R.A. Boudreau and R.D. Rauh, *Sol. Energy Mater.*, **7**, 385 (1982).
    (c) Y. Mirovsky, R. Tenne, G. Hodes and D. Cahen, *Thin Solid Films*, **91**, 349 (1982).
    (d) D. Cahen, G. Hodes and J. Manassen, *Nature (London)*, **261**, 403 (1976).
11. (a) B. Miller, A. Heller, M. Robbins, S. Menezes, K.C. Chang and J. Thompson, Jr., *J. Electrochem. Soc.*, **124**, 1019 (1977).
    (b) R.N. Noufi, P.A. Kohl and A.J. Bard, *J. Electrochem. Soc.*, **125**, 375 (1978).
12. (a) J.W. Matthews, *Epitaxial Growth*, Academic Press, New York, 1975, Part A.
    (b) L. Aleksandrov, *Growth of Crystalline Semiconductor Materials on Crystal Surfaces*, Elsevier, Amsterdam, 1984.
    (c) R.A. Laudise, *The Growth of Single Crystals*, Prentice-Hall, Englewood Cliffs, N.J., 1970.
13. J. Kiwi, K. Kalyanasundaram and M. Gratzel, in *Structure and Bonding*, K. Jorgensen, Ed., Springer-Verlag, Berlin, 1982.
14. (a) H.O. Finklea, *Semiconductor Electrodes*, Elsevier, Amsterdam, 1988.
    (b) Yu.V. Pleskov and Yu.Ya. Guervich, *Semiconductor Photoelectrochemistry*, translated from Russian by Consultants Bureau, New York, 1986.
15. H. Landolt and R. Bornstein, *Numerical Data and Fundamental Relationships in Science and Technology*, Vol. 17, *Semiconductors*, O. Madelung, M. Schule and H. Weiss, Eds., Springer-Verlag, Berlin, 1982.
16. A. Many, Y. Goldstein and N.B. Grover, *Semiconductor Surfaces*, North-Holland, New York, 1965.
17. (a) C.M. Gronet, N.S. Lewis, G. Cogan and J. Gibbons, *Proc. Natl. Acad. Sci. USA*, **80**, 1152 (1983).
    (b) J.A. Bruce and M.S. Wrighton, *J. Electroanal. Chem.*, **122**, 93 (1981).
18. B.A. Parkinson, A. Heller and B. Miller, *J. Electrochem. Soc.*, **126**, 954 (1979).
19. H.J. Lewerenz, D.E. Aspnes, B. Miller, D.L. Malm and A. Heller, *J. Am. Chem. Soc.*, **104**, 3325 (1982).
20. R. Tenne and G. Hodes, *Appl. Phys. Lett.*, **37**, 428 (1980).

21. J. Mandelkorn and J.H. Lamneck, Jr., *Proc. 9th IEEE Photovoltaic Spec. Conf.*, **9**, 83 (1972).
22. K. Rajeshwar and M. Kanek, *J. Phys. Chem.*, **89**, 3588 (1985).
23. (a) D.E. Aspnes and A. Heller, *J. Phys. Chem.*, **87**, 4919 (1983).
    (b) A. Heller, E. Aharon-Shalom, W.A. Bonner and B. Miller, *J. Am. Chem. Soc.*, **104**, 6942 (1982).
24. W.G. Moffatt, G.W. Pearsall and J. Wulff, *Structure*, Wiley, New York, 1964.
25. (a) E.H. Poindexter, P.J. Caplan, B.E. Deal and R.R. Razouk, *J. Appl. Phys.*, **52**, 879 (1981).
    (b) P.J. Caplan, E.H. Poindexter, B.E. Deal and R.R. Razouk, *J. Appl. Phys.*, **50**, 5847 (1979).
26. (a) W.H. Laflere, F. Cardon and W.P. Gomes, *Surf. Sci.*, **59**, 401 (1976).
    (b) J.L. Richards and A.J. Crocker, *J. App. Phys.*, **31**, 611 (1960).
27. (a) R.H. Bube, *Electronic Properties of Crystalline Solids*, Academic Press, New York, 1974.
    (b) R.H. Bube, *Photoconductivity of Solids*, R.E. Krieger, Huntington, N.Y., 1978.
28. D.A. Aspnes and A.A. Studna, *Phys. Rev. B*, **27**, 985 (1983).
29. (a) S.M. Sze and J.C. Irvin, *Solid-State Electron.*, **11**, 599 (1968).
    (b) W.R. Thurber, R.L. Mattis and Y.M. Liu, *J. Electrochem. Soc.*, **127**, 2293 (1980).
30. L.J. Van der Pauw, *Philips Res. Rep.*, **13**, 1 (1958).
31. J.R. Haynes and W. Shockley, *Phys. Rev.*, **81**, 835 (1951).
32. L.C. Feldman and J.W. Mayer, *Fundamentals of Surface and Thin Film Analysis*, Elsevier, New York, 1986.
33. M.A. Van Hove, W.H. Weinberg and C.-M. Chan, *Low Energy Electron Diffraction*, Springer-Verlag, Berlin, 1986.
34. (a) G. Binnig, H. Rohrer, Ch. Gerber and E. Weibel, *Phys. Rev. Lett.*, **49**, 57 (1982).
    (b) G. Binnig and H. Rohrer, *IBM J. Res. Dev.*, **30**, 355 (1986).
    (c) G. Binnig and H. Rohrer, *Surf. Sci.*, **26**, 236 (1983).
    (d) J.A. Golovchenko, *Science*, **232**, 48 (1986).
35. (a) R.M. Feenstra, J. Tersoff and A.P. Fein, *Phys. Rev. Lett.*, **58**, 1192 (1987).
    (b) R.M. Feenstra, J.A. Stroscio and A.P. Fein, *Surf. Sci.*, **181**, 295 (1987).
36. R. Sinclair, F. Ponce, T. Yamashita and J. Bravman, *Proc. 39th Annu. Conf. EMSA*, **39**, 124 (1981).
37. D.C. Koningsberger and R. Prins, *X-Ray Absorption: Principles, Applications, Techniques of EXAFS, SEXFAS, and XANES*, Wiley, New York, 1988.
38. (a) O.R. Melroy et al., *Langmuir*, **4**, 728 (1988), and references therein.
    (b) C. Levy-Clement, J. Rioux, J.R. Dahn and W.R. McKinnon, *Mater. Res. Bull.*, **19**, 1629 (1984).
39. (a) P. Skeath, I. Lindau, P.W. Chye, C.Y. Su and W.E. Spicer, *J. Vac. Sci. Technol.*, **16**, 1143 (1979).
    (b) P.E. Gregory and W.E. Spicer, *Phys. Rev. B*, **13**, 725 (1976).
40. W.E. Spicer, "The Use of Synchrotron Radiation in UPS: Theory and Results," in *Electron and Ion Spectroscopy of Solids*, L. Fiermans, J. Vennik and W. Dekeyser, Eds. (NATO ASI Series B, Vol. 32), Plenum Press, New York, 1978.
41. H. Gerischer, *J. Electroanal. Chem.*, **58**, 263 (1975).
42. (a) S.R. Morrison, *The Chemical Physics of Surfaces*, Plenum Press, New York, 1977.
    (b) E.H. Nicollian and A. Goetzberger, *Appl. Phys. Lett.*, **7**, 216 (1965).
    (c) E.H. Nicollian and A. Goetxberger, *Bell Syst. Tech. J.*, **46**, 1055 (1967).
43. S. Tanaka, J.A. Bruce and M.S. Wrighton, *J. Phys. Chem.*, **85**, 3778 (1981).
44. (a) R.P. Silberstein and F.H. Pollak, *J. Vac. Sci. Technol.*, **17**, 1052 (1980).
    (b) P. Lemasson, J.P. Dalbera and J. Gautron, *J. Appl. Phys.*, **52**, 6296 (1981).
    (c) R.P. Silberstein, J.K. Lyden, M. Tomkiewicz and F.H. Pollak, *J. Vac. Sci. Technol.*, **19**, 406 (1981).

45. (a) D.E. Aspnes and A.A. Studna, *Phys. Rev. B*, **7**, 4605 (1973).
(b) A.G. Thompson, M. Gardona, K.L. Shaklee and J.C. Wooley, *Phys. Rev.*, **146**, 601 (1966).
46. ASTM F391-78, *1979 Annual Book of ASTM Standards*, **43**, 770 (1979).
47. A. Moore, *Appl. Phys. Lett.*, **40**, 403 (1981).
48. E. Yablanovitch, C.J. Sandroff, R. Bhat and T. Gmitter, *Appl. Phys. Lett.*, **51**, 439 (1987).
49. E. Yablanovitch, R.M. Swanson, W.D. Eades and B.R. Weinberger, *Appl. Phys. Lett.*, **48**, 245 (1986).
50. (a) M.D. Fayer, *Annu. Rev. Phys. Chem.*, **33**, 63 (1982).
(b) K.A. Nelson, R. Casalegno, R.J.D. Miller and M.D. Fayer, *J. Chem. Phys.*, **77**, 1144 (1982).
51. J. Vaitkus, *Phys. Status Solidi*, **34**, 769 (1976).
52. (a) A.E. Dixon, D.F. Williams, S.R. Das and J.B. Webb, *J. Appl. Phys.*, **57**, 2963 (1985).
(b) H.K. Kiuken and C. van Opdorp, *J. Appl. Phys.*, **57**, 2077 (1985).
(c) H.J. Leamy, *J. Appl. Phys.*, **53**, R51 (1982).
(d) W.D. Johnston, Jr., H.J. Leamy, B.A. Parkinson, A. Heller and B. Miller, *J. Electrochem. Soc.*, **127**, 90 (1980).
53. (a) H.U. Harten, *Philips Res. Rep.*, **14**, 346 (1959).
(b) H.U. Harten, *J. Phys. Chem. Solids*, **14**, 220 (1960).
54. (a) M.A. Butler and D.S. Ginley, *J. Electrochem. Soc.*, **128**, 712 (1981).
(b) J.-N. Chazalviel, *J. Electrochem. Soc.*, **127**, 1822 (1980).
(c) D.N. Rose, Y. Ramprakash and S. Basu, *J. Electrochem. Soc.*, **131**, 850 (1954).